POWER HANDLING CHALLENGES OF HIGH K_T^2 ALSCN LAMB WAVE RESONATORS

Mingyo Park[1], Yue Zheng[1], and Azadeh Ansari[1]*
[1]Georgia Institute of Technology, Atlanta, Georgia, USA

ABSTRACT

This work reports on the first demonstration of a first-order symmetric (S_1) mode Lamb-wave resonator (LWR) based on sputtered $Al_{1-x}Sc_xN$ (x~%30), with a large electromechanical coupling coefficient (k_t^2) up to 13.7%, and frequencies in the range of 340 MHz up to 9.9 GHz. To fulfill the high-power requirements for today's radio frequency applications, we introduced a comprehensive study on the characterization of the resonator nonlinearity depending on device Q, and the power-handling capability based on different Sc/(Sc+Al) ratios and thermal conductivities. Additionally, we report the highest k_t^2 AlN-based LWRs of 13.7% and bode Q of 334 at 2.7GHz. This work shows the first study of 1-dB gain compression point vs. Sc/(Al+Sc).

KEYWORDS

Acoustic resonators/filters, Lamb-wave resonators, First-order symmetric (S_1) mode, Aluminum scandium nitride, Electromechanical coupling coefficient, Power handling capability, 1-dB gain compression point, Duffing nonlinearity, Thermal conductivity.

INTRODUCTION

Multiple passbands radio frequency (RF) filters meet the needs of miniaturization and integration for fifth-generation new radio (5G NR) communications. Lamb-wave resonators (LWRs) are widely studied for implementation in RF front-end modules. Compared to film bulk acoustic resonators (FBARs), LWRs offer single-chip, multi-frequency, multi-band solutions with flexibility over the interdigitated transducer pitch/geometry defined by lithography [1], [2]. Compared to Rayleigh surface acoustic wave (SAW) resonators, LWRs enable higher frequencies and larger quality factor (Q) and electromechanical couplings (k_t^2) by taking advantage of high overtone modes (i.e., A_1 and S_1), and higher phase velocities with better acoustic wave confinement in the piezoelectric-layer [3]–[6]. Aluminum Scandium Nitride ($Al_{1-x}Sc_xN$) has been popular in the acoustic community in recent years [7]–[9], showing enhanced piezoelectricity to compensate for pure AlN's moderate k_t^2, an essential metric for acoustic devices to determine the filter's fractional bandwidth. In addition to Q, the insertion loss, and bandwidth, wireless communication devices call for high-performance filters that offer enhanced power-handling capability and less intermodulation distortion for filter band/channel selection [8]-[9].

Emerging RF power requirements have increased the overall system heating. In order to maintain device reliability and performance, filters must be able to handle high power levels and efficiently dissipate the additional heat. Several factors limit the power-handling ability of RF filters, including self-heating, which leads to thermal breakdown, and device nonlinearities that affect the filter transfer response. Given the high-power operation requirements in 5G, the high-temperature study of acoustic resonators is critical due to the self-heating of the device under high power operation [12]. Our group has previously studied the thermal conductivity (TC) of AlN and AlScN films [13] and reported that AlScN shows significantly lower TC than pure AlN, which can lead to severe self-heating [12], [13]. The lower TC challenges the power handling of the device, showing a tradeoff of k_t^2. Therefore, characterizing the power-handling of AlScN-based resonators needs to be studied for high-power RF applications.

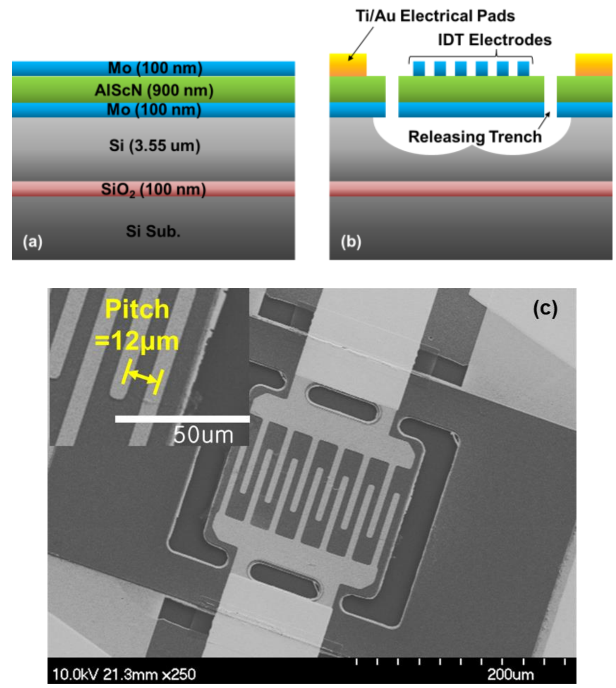

Figure 1: Cross-sectional schematic of (a) initial sample with the sputtered deposited Mo(100 nm)/AlScN(900 nm)/Mo(100 nm) on SOI substrate and (b) fabricated LWR released from the front side with isotropic etching of the 3.55 um-thick Si device layer. (c) SEM image of AlScN LWR with 12 um IDT pitches.

In this work, we report on the first demonstration of first-order symmetric (S1) LWR based on $Al_{0.7}Sc_{0.3}N$, with high phase velocities and large k_t^2 [3], presenting frequencies as high as 9.9GHz and k_t^2 values up to 13.7%. We take advantage of the enhanced k_t^2 by using 30% Sc/(Al+Sc) ratio in AlScN films, as well as utilizing a bottom electrode (BE) as the ground electrode. Here, we report the highest k_t^2 AlN-based LWRs of 13.7% and bode Q [5] of 334 at 2.7GHz. The resonator nonlinearity is evaluated based on the Q of the device under driving power levels in terms of peak frequency shift. The power-handling capability is analyzed based on different Sc/(Sc+Al) ratios and TC values, showing a reduction of P1dB at higher Sc/(Al+Sc) ratios. This work is the first study of P1dB vs. Sc/(Al+Sc).

FABRICATION PROCESS

LWRs with the resonant stack of molybdenum (Mo)/$Al_{0.7}Sc_{0.3}N$/Mo and thicknesses of 100 nm/900 nm/100 nm, respectively, are sputter-deposited on a silicon-on-insulator (SOI) substrate at VTT Technical Research Centre of Finland. Figure 1 shows a cross-sectional schematic of (a) the initial sample wafer stack and (b) fabricated LWR. The fabrication process is started by

978-1-940470-04-7/HH2022/$25©2022TRF
DOI 10.31438/trf.hh2022.13

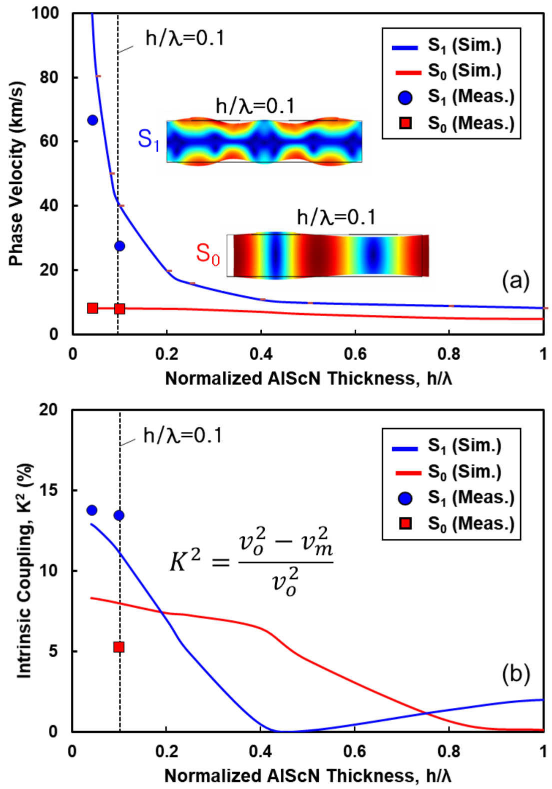

Figure 2: (a) Phase velocity and (b) Intrinsic coupling (K^2) of FEA simulation and measured data points of LWR S0, and S1 modes based on normalized $Al_{0.7}Sc_{0.3}N$ thickness (h/λ), along with mode shapes at h/λ=0.1 without electrode.

etching down the top Mo layer with reactive ion etching (RIE) under SF_6-based chemistry to pattern interdigital transducer (IDT) electrodes. The $Al_{0.7}Sc_{0.3}N$ piezoelectric layer is etched via an inductively coupled plasma (ICP) ion-etching tool with chlorine-based chemistry. The device is released from the Si device layer by being exposed to xenon difluoride (XeF2) Si etcher through releasing trenches. Figure 1 (c) illustrates the scanning electron microscope (SEM) image of the fabricated 12µm-pitched LWR released from the front side.

$AL_{0.7}SC_{0.3}N$ LAMB WAVE RESONATORS DESIGN

Resonator Electromechanical Characterization

Figure 2 is simulated with finite element analysis (FEA) using the evaluated piezoelectric coefficient and elastic constants, including Sc/(Al+Sc) ratio of 30% [7] to characterize dispersion curves of two different symmetric modes (S_0 and S_1). Figure 2 illustrates the simulated phase velocity and intrinsic coupling (K^2) of S_0 and S_1 LWR with BE based on normalized $Al_{0.7}Sc_{0.3}N$ thickness (h/λ), plotted with measured data points. Figure 2(a) describes the excited two resonance modes along with the displacement mode shape at h/λ=1, showing the symmetric deformation shape in the piezoelectric layer.

The K^2 is calculated based on the phase velocity of the electrically free piezo-layer surface (v_o) and the shorted surface (v_m). As shown in Figure 2, the higher-order LW mode shows better K^2 and much higher phase velocities, particularly when the film thickness is thin relative to wavelength (h/λ<0.4).

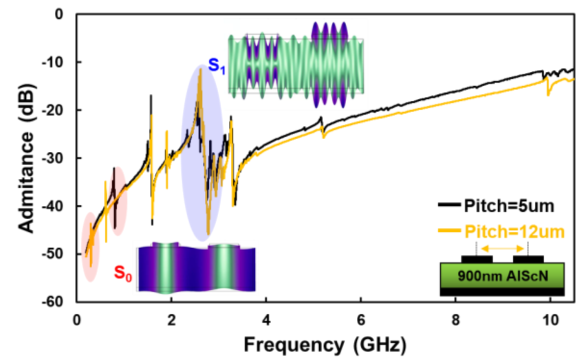

Figure 3: Measured admittance frequency response with the frequency range from 0.2 to 10.5 GHz of 5 um and 12 um-pitched $Al_{0.7}Sc_{0.3}N$ LWR showing multi-resonance modes along with the mode shapes including 100 nm-thick top and bottom Mo electrodes.

Table 1: Device performance of S_0 and S_1 modes at h/λ=0.1 and 0.04.

h/λ	Mode	f_r (GHz)	k_t^2 (%)	Q_{bode}	Phase (km/s)
0.1	S0	0.79	5.2	104	7.9
0.1	S1	2.59	13.4	274	27.4
0.04	S0	0.34	2.12	189	8.3
0.04	S1	2.62	13.7	334	66.8

Experimental Frequency Response and Resonant Mode Characteristic of Lamb Wave Resonators

The proposed LWRs are measured in an RF probe station, and resonance characteristic curves are tested by an Agilent N5224B Network Analyzer after performing a short-open-load-through (SOLT) calibration. Figure 3 demonstrates the measured wideband admittance frequency response of 5 µm and 12 µm-pitched devices with a frequency ranging from 0.2 to 10.5 GHz.

In the wideband frequency response, LWR shows a multi-resonant frequency response with various modes, including undesired spurious modes. The difference in resonance frequency is observed from the S_0 mode between 5 µm and 12 µm-pitched devices due to different wavelengths (λ) followed by the definition of resonance frequency (f=v/λ) [14]. On the other hand, similar resonance frequencies are observed from S_1 mode between 5 µm and 12 µm-pitched devices. Since the phase velocity of the S_1 LW mode is more dispersive than the S_0 mode, a larger phase velocity below h/λ<0.4 compensates decrease in frequency caused by a larger wavelength. The highest measured phase velocity of S_1 mode is 66800m/s, more than 8 times larger than the phase velocity of S_0 mode at h/λ=0.04.

The electromechanical coupling coefficient (k_t^2) is defined by the following equation [14], [15]:

$$k_t^2 = \frac{\pi^2}{4} \times \frac{f_s(f_p - f_s)}{f_p^2} \quad (1)$$

Where f_s is the series and f_p is the parallel resonant frequency determined from the measured admittance (Y_{11})-parameter of the device. The Q of LWR is analyzed by bode Q based on the measured phase group delay of the S-parameter [7]. Table I summarizes the evaluated device performance of S_0 and S_1 LWR in $Al_{0.7}Sc_{0.3}N$ films. The highest k_t^2 of 13.7% and bode Q of 334 can be achieved at the resonant frequency of 2.7 GHz, yielding a $Q \times k_t^2$ figure of merit

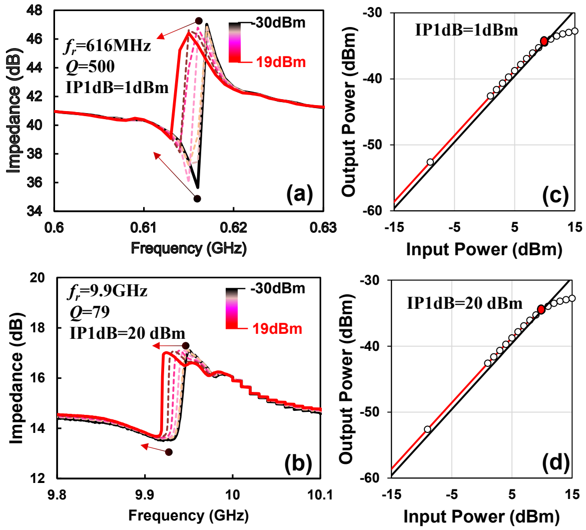

Figure 4: Measured impedance with the power sweep range from -30 to 19dBm on resonance mode with (a) Q of 500 including (c) measured P1dB=1dBm and (b) Q of 79 including (d) measured input P1dB=20dBm, showing duffing nonlinearity at high power.

(FoM) of 45.7. Such a result is 9 times larger than FoM of 5.4 in S_0 LWR at the resonant frequency of 790 MHz. Thus, elaborating higher-order LW modes can lead to a higher frequency filter solution without compromising other key performance parameters.

DEVICE POWER CHARACTERISTICS AND EXPERIMENTAL RESULTS

Device Nonlinearity based on the Quality Factor

Figure 4 demonstrates the power measurement of the $Al_{0.3}Sc_{0.7}N$ LW device. Figure 4 (a)-(b) show the measured impedance (Z-parameter) of two resonance modes at the resonance frequency of 616 MHz and 9.9 GHz by a sweeping power range of -30 dBm to 19 dBm. Duffing nonlinearity is commonly observed when the input signal of sufficiently high power gives rise to access to the nonlinear regime. The devices and materials exhibit various stiffness phases to exploit their chaotic motion in nonlinear systems showing the softening or hardening effect in the mode [16]. As increase the input power, Duffing effect induces a resonant frequency shift due to softening effect in mode, as presented in Figure 4 (a)-(b).

Furthermore, in order to characterize device power handling capability, gain compression point (P1dB) is measured as shown in Figure 4 (c)-(d). The standard setup for P1dB testing involves 2-port terminals, and each port is connected to a signal generator as the input and a spectrum analyzer as the output. The signal generator frequency is adjusted to the targetted resonance frequency, and the output power is swept to explore the 1-dB compression point.

Figure 4 shows the characterization of the resonator nonlinearity depending on device *Q*. Compared to the low *Q* (=79) resonance mode with input P1dB of 20 dBm, a relatively poor power-handling of 1 dBm is observed in the high *Q* (=500) resonance mode showing more intense Duffing nonlinearity as power increases. Such results prove that power handling capability is challenged in high *Q* devices because of device nonlinearity.

Impact of Thermal conductivity on Power Handling Capability

Recent study [17] report on the correlation between $Al_{1-x}Sc_xN$ thermal conductivity and (1) x% in $Al_{1-x}Sc_xN$, and (2) $Al_{1-x}Sc_xN$ thickness to analyze overheating of piezoelectric film which limits power handling capability of the device. Figure 5 (a) [13] describes measured thermal conductivity with a fitted curve based on Sc concentration, presenting a decreasing trend in thermal conductivity with increasing Sc. For example, the 400 nm-thick pure AlN provides a 30 times decreased thermal conductivity than 400 nm-thick $Al_{0.74}Sc_{0.26}N$ [13]. In terms of thermal conductivity values depending on film thickness, a higher thermal conductivity value is observed in thicker $Al_{1-x}Sc_xN$ films [17].

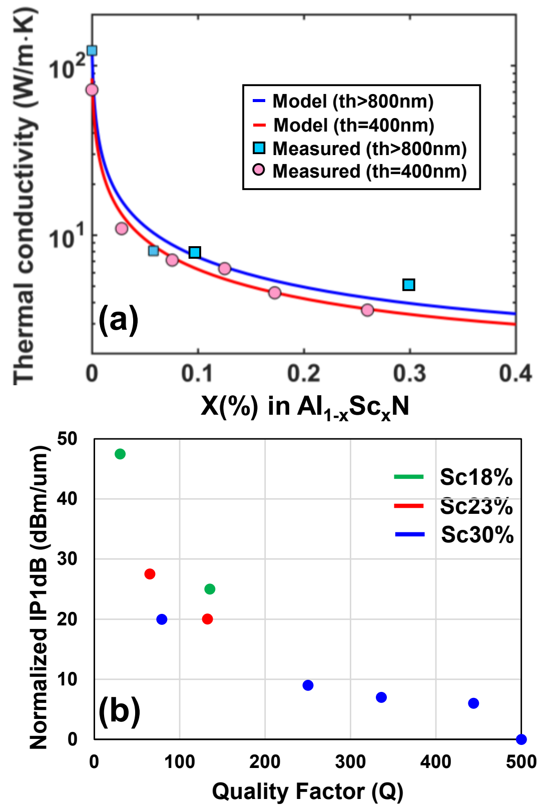

Figure 5: (a) Measured and fitted thermal conductivity curve based on x= Sc/(Al+Sc) for $Al_{1-x}Sc_xN$ thickness (th) of th=400nm and th>800 nm films. (b) Measured normalized input power 1dB compression point (IP1dB) based on Q of $Al_{1-x}Sc_xN$ device with x=18, 23, 30%.

Based on this behavior, this work analyzes the power handling capability is analyzed based on different Sc/(Sc+Al) ratios and their corresponding thermal conductivity values. Figure 5 (b) shows the measured input power P1dB based on *Q* and Sc/(Al+Sc) ratio. Input P1dB is normalized by AlScN thickness considering the effects of power handling on film thickness [18], [19]. LW devices based on $Al_{1-x}Sc_xN$ film with various x=18, 23, 30% are measured and evaluated in compliance with the effects of the *Q* of each device. Normalized input P1dB shows a decreasing trend as *Q* increases caused by device nonlinearity due to high *Q*.

Moreover, input P1dB presents a decreasing trend as Sc/(Al+Sc) increases due to low thermal conductivity in accordance with high x in $Al_{1-x}Sc_xN$ film. Table 2 summarizes the previous LWRs and this work. To the best of the authors' knowledge, this work shows the highest k_t^2 (=13.7 %) of any AlN-based S_1 mode LWR reported up to date.

Table 2: Comparison table of LWR device metrics of previous work and our work.

	$\frac{Sc}{Sc+Al}$ (%)	M*	f_r (GHz)	k_t^2 (%)	Q	IP1dB (dBm)
[10]	0	S_0	1.5	NA	1500	25
[10]	0	S_1	0.2	1.4	1225	20
[4]	0	S_0	3.5	3.59	550	NA
[3]	0	S_1	1.38	0.71	2181	NA
[9]	32	S_0	0.04	10.2	700	NA
This Work	30	S_1	2.6	13.7	334	5.5

M : Mode*

CONCLUSION

High power handling is a crucial requirement for today's RF filter and duplexer applications. Lamb-wave resonator with higher-order modes is one of the alternative technologies to offer solutions to a growing high power market, providing single-chip, high resonant frequency, and multi-frequency RF modules without degrading the filter's FoM.

In this work, we presented a comprehensive study on the characterization of the power-handling of AlScN-based resonators for high-power RF applications. The resonator nonlinearity is evaluated based on Q, and the power-handling capability is analyzed based on different Sc/(Sc+Al) ratios and TC values, showing a decrease of P1dB at higher Sc/(Al+Sc) ratios. We report on the first demonstration of first-order symmetric (S1) LWR based on $Al_{0.7}Sc_{0.3}N$, with high phase velocities of 66800m/s and large k_t^2 up to 13.7%, presenting frequencies as high as 9.9GHz. To the best of the authors' knowledge, we report the highest k_t^2 AlN-based LWRs of 13.7% and bode Q of 334 at 2.7GHz. Furthermore, this work is the first study of P1dB vs. Sc/(Al+Sc).

ACKNOWLEDGEMENTS

The authors would like to acknowledge the VTT Technical Research Centre of Finland for providing the wafer.

REFERENCES

[1] H. Campanella, Y. Qian, C. O. Romero, J. S. Wong, J. Giner, and R. Kumar, "Monolithic Multiband MEMS RF Front-End Module for 5G Mobile," J. Microelectromechanical Syst., vol. 30, no. 1, pp. 72–80, 2021, doi: 10.1109/JMEMS.2020.3036379.

[2] M. Park, J. Wang, R. Dargis, A. Clark, and A. Ansari, "Super High-Frequency Scandium Aluminum Nitride Crystalline Film Bulk Acoustic Resonators," in 2019 IEEE International Ultrasonics Symposium (IUS), Oct. 2019, pp. 1689–1692, doi: 10.1109/ULTSYM.2019.8925598.

[3] J. Zou et al., "Spectrum-clean S1 AlN Lamb wave resonator with damped edge reflectors Spectrum-clean S1 AlN Lamb wave resonator with damped edge reflectors," Appl. Phys. Lett., vol. 116, no. 2, Dec. 2019, doi: 10.1063/1.5128961.

[4] A. Gao, J. Zou, and S. Gong, "A 3.5 GHz AlN S1 lamb mode resonator," 2017 IEEE International Ultrasonics Symposium (IUS), Sep. 2017, doi: 10.1109/ULTSYM.2017.8092161.

[5] A. Kourani, Y. Yang, and S. Gong, "A Ku-Band Oscillator Utilizing Overtone Lithium Niobate RF-MEMS Resonator for 5G," IEEE Microw. Wirel. Components Lett., vol. 30, no. 7, pp. 681–684, Jul. 2020, doi: 10.1109/LMWC.2020.2996961.

[6] J. Zou, C. M. Lin, Y. Y. Chen, and A. P. Pisano, "High-frequency and low-resonance-impedance lamb wave resonators utilizing the S1 mode," 2015 Transducers - 2015 18th Int. Conf. Solid-State Sensors, Actuators Microsystems, TRANSDUCERS, pp. 2025–2028, Jun. 2015, doi: 10.1109/TRANSDUCERS.2015.7181353.

[7] M. Park, Z. Hao, R. Dargis, A. Clark, and A. Ansari, "Epitaxial Aluminum Scandium Nitride Super High Frequency Acoustic Resonators," J. Microelectromechanical Syst., vol. 29, no. 4, pp. 490–498, Aug. 2020, doi: 10.1109/JMEMS.2020.3001233.

[8] M. Park, J. Wang, and A. Ansari, "High-Overtone Thin Film Ferroelectric AlScN-on-Silicon Composite Resonators," IEEE Electron Device Lett., vol. 42, no. 6, pp. 911–914, 2021, doi: 10.1109/LED.2021.3070274.

[9] G. Esteves et al., "Al0.68Sc0.32N Lamb wave resonators with electromechanical coupling coefficients near 10.28%," Appl. Phys. Lett., vol. 118, no. 17, pp. 0–5, 2021, doi: 10.1063/5.0047647.

[10] H. Campanella, M. Narducci, N. Wang, J. Bo, and W. Soon, "RF-Designed High-Power Lamb-Wave Aluminum – Nitride Resonators," IEEE Transaction on Microwave Theor and Techniques, vol. 63, no. 2, pp. 331–339, Feb. 2015.

[11] H. Campanella, L. Khine, and J. M. Tsai, "Aluminum nitride lamb-wave resonators for high-power high-frequency applications," IEEE Electron Device Lett., vol. 34, no. 2, pp. 316–318, 2013, doi: 10.1109/LED.2012.2230609.

[12] C. Yuan at al., "Phonon heat conduction in Al 1-x Sc x N thin films," in Materials Today Physics, vol. 21, 200498, pp. 1–19, 2021.

[13] Y. Zheng, M. Park, A. Ansari, C. Yuan, and S. Graham, "Self-Heating and Quality Factor: Thermal Challenges in Aluminum Scandium Nitride Bulk Acoustic Wave Resonators," 21st Int. Conf. Solid-State Sensors, Actuators Microsystems, TRANSDUCERS 2021, pp. 321–324, Jun. 2021, doi: 10.1109/Transducers50396.2021.9495613.

[14] M. Park, Z. Hao, D. G. Kim, A. Clark, R. Dargis, and A. Ansari, "A 10 GHz Single Crystalline Sc-AlN Lamb-wave Resonator," 2019 20th International Conference on Solid-State Sensors, Actuators and Microsystems & Eurosensors XXXIII, Jun. 2019, doi: 10.1109/TRANSDUCERS.2019.8808374.

[15] M. Park and A. Ansari, "Epitaxial Al0.77Sc0.23N SAW and Lamb Wave Resonators," in IFCS-ISAF 2020 - Joint Conference of the IEEE International Frequency Control Symposium and IEEE International Symposium on Applications of Ferroelectrics, Jul. 2020, doi: 10.1109/IFCS-ISAF41089.2020.9234850.

[16] R. Lu and S. Gong, "Study of thermal nonlinearity in lithium niobate-based MEMS resonators," 2015 Transducers - 2015 18th Int. Conf. Solid-State Sensors, Actuators Microsystems, TRANSDUCERS 2015, pp. 1993–1996, 2015, doi: 10.1109/TRANSDUCERS.2015.7181345.

[17] Y. Song et al., "Thermal Conductivity of Aluminum Scandium Nitride for 5G Mobile Applications and beyond," ACS Appl. Mater. Interfaces, vol. 13, no. 16, pp. 19031–19041, 2021, doi: 10.1021/acsami.1c02912.

[18] N. Klein et al., "Microwave properties of MgB2 thin films," IEEE Trans. Appl. Supercond., vol. 13, no. 2, pp. 3253–3256, 2003, doi: 10.1109/TASC.2003.812214.

[19] A. Leon et al., "RF power-handling performance for direct actuation of germanium telluride switches," IEEE Trans. Microw. Theory Tech., vol. 68, no. 1, pp. 60–73, 2020, doi: 10.1109/TMTT.2019.2946145.

CONTACT

*M. Park; m.park@gatech.edu